

**Vertical correlation and miniband formation in submonolayer Zn(Cd)Te/ZnCdSe type-II quantum dots for intermediate band solar cell application**

S. Dhomkar, U. Manna, I. C. Noyan, M. C. Tamargo, and I. L. Kuskovsky

Citation: *Applied Physics Letters* **103**, 181905 (2013); doi: 10.1063/1.4827636

View online: <http://dx.doi.org/10.1063/1.4827636>

View Table of Contents: <http://scitation.aip.org/content/aip/journal/apl/103/18?ver=pdfcov>

Published by the **AIP Publishing**

---

**Advertisement:**



**Goodfellow**

metals • ceramics • polymers  
composites • compounds • glasses

**Save 5% • Buy online**  
70,000 products • Fast shipping

## Vertical correlation and miniband formation in submonolayer Zn(Cd)Te/ZnCdSe type-II quantum dots for intermediate band solar cell application

S. Dhomkar,<sup>1,2,a)</sup> U. Manna,<sup>3</sup> I. C. Noyan,<sup>3</sup> M. C. Tamargo,<sup>2,4</sup> and I. L. Kuskovsky<sup>1,2,b)</sup>

<sup>1</sup>Department of Physics, Queens College of CUNY, Queens, New York 11367, USA

<sup>2</sup>The Graduate Center, CUNY, New York, New York 10016, USA

<sup>3</sup>Department of Applied Physics and Applied Mathematics, Columbia University, New York, New York 10027, USA

<sup>4</sup>Department of Chemistry, City College of CUNY, New York, New York 10031, USA

(Received 25 August 2013; accepted 16 October 2013; published online 29 October 2013)

High resolution x-ray diffraction based reciprocal space mapping is employed to investigate vertical correlation in submonolayer Zn(Cd)Te/ZnCdSe type-II quantum dots (QDs). The average lateral deviation from one dot to another is found to decrease from 13%–17% to 8%–11% with an increase in QD size. Narrower photoluminescence with a better yield is obtained for the sample with improved vertical correlation, indicating smaller QD size distribution along with partial suppression of non-radiative recombination paths. Observed reduction in radiative lifetimes and supportive calculations demonstrate enhanced hole-hole wavefunction overlap pointing towards possibility of miniband formation, an advantageous feature for an intermediate band solar cell. © 2013 AIP Publishing LLC. [<http://dx.doi.org/10.1063/1.4827636>]

The concept of intermediate band (IB) solar cells<sup>1</sup> (SCs) offers a promising approach to raise the limiting efficiency of a conventional solar cell<sup>2,3</sup> to 63.2%<sup>1,4–6</sup> under full solar concentration. IB-SCs consist of an active material having a band of states within the band gap of the host semiconductor to enhance the two- (or more) photons absorption process, thereby improving the photocurrent significantly, while preserving the open circuit voltage. A miniband is a desired attribute for an efficient IB-SC, first to increase the below band gap absorption by increasing the density of states and second, to avoid the effects of the Shockley-Read-Hall non-radiative recombination,<sup>7</sup> which gets amplified due to presence of localized states. The IB, in principle, can be engineered by means of quantum dots (QDs);<sup>5,6</sup> however, well studied systems such as type-I InAs/GaAs QDs,<sup>8,9</sup> have far from ideal material parameters<sup>5,6</sup> and pose problems like presence of low barriers with wetting layers,<sup>5</sup> strain induced dislocations,<sup>10</sup> and inferior performance due to high carrier recombination rates.<sup>11,12</sup> Thus, to overcome some of these issues, we have recently proposed a material system based on submonolayer Zn(Cd)Te/ZnCdSe type-II QDs.<sup>13,14</sup> It has been shown that this system has appropriate material parameters and hundreds of layers with embedded QDs formed without detrimental wetting layers can be grown via migration enhanced epitaxy (MEE). Additionally, type-II band alignment is supposed to avoid undesired voltage reduction<sup>15</sup> and assist in the carrier extraction process<sup>11</sup> due to reduced radiative recombination within QDs as well as due to suppression of non-radiative Auger recombination,<sup>16</sup> owing to spatially indirect nature of the excitons.<sup>17</sup>

In this article, we show that a miniband can indeed be fabricated as a result of enhanced vertical correlation within

the Zn(Cd)Te/ZnCdSe QD superlattices (SLs) with relatively large QDs separated by a thin spacer region. Also, vertical correlation is highly beneficial for obtaining uniform QDs with improved structural properties. Moreover, submonolayer QDs, and particularly those under investigation, are hard to image due to their submonolayer nature and very low contrast between the host and the QD forming materials. Additionally, non-destructive techniques requiring minimal sample preparation are always desirable for structural analysis. Hence, high resolution x-ray diffraction (HRXRD) based reciprocal space maps (RSMs) have been utilized to investigate the structural properties and spatial correlation of the submonolayer QDs, while continuous-wave (CW-) and time-resolved (TR-) photoluminescence (PL) was employed to confirm type-II band alignment and to investigate miniband formation.

The HRXRD measurements were carried out at Beamline X20A at the National Synchrotron Light Source at the Brookhaven National Laboratory. All measurements were performed using monochromatic synchrotron radiation at 8 keV with a double-crystal Ge (111) monochromator. To enhance the angular resolution, a Ge (111) analyzer was placed in front of the detector. For CW-PL and TR-PL measurements samples were placed inside a Janis Research closed cycle refrigerating system. For CW-PL studies, the 351 nm emission line from an Ar<sup>+</sup> laser was used as an excitation source, while TR-PL measurements were performed using the 337 nm line of a N<sub>2</sub> pulsed laser with 4 ns pulse width. The excitation intensity was varied by over four orders of magnitude using neutral density filters. The signal was dispersed through a third stage of a TriVista SP2 500i triple monochromator and was detected by a thermoelectrically cooled GaAs photomultiplier tube. The TR-PL signal was recorded using a 500 MHz Tektronix TDS 654C oscilloscope.

Two samples (referred here as A and B) were grown by varying Te flux during MEE cycles and with a spacer

<sup>a)</sup>Electronic mail: sdhomkar@qc.cuny.edu

<sup>b)</sup>Electronic mail: Igor.Kuskovsky@qc.cuny.edu

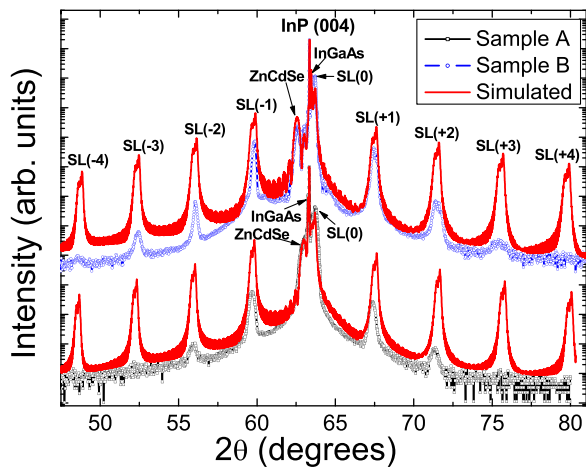


FIG. 1. Experimental and simulated  $\omega$ - $2\theta$  curves along (004) orientation for samples A and B.

thickness of  $\sim 2.7$  nm, under same growth conditions as that of sample D in Ref. 13. The periodic satellite SL peaks shown in Fig. 1 confirmed high crystalline quality of the samples, while intensity dependent CW-PL and TR-PL confirmed type-II nature of the multilayered structure (not shown here). The  $\omega$ - $2\theta$  curves were then simulated using a BEDE RADS program based on Takagi<sup>18</sup> and Taupin<sup>19</sup> generalized dynamical theory to extract the structural parameters.

Initial parameters required for the simulation, such as spacer compositions, thicknesses, and strain, were obtained from various HRXRD scans along symmetric as well as asymmetric reflections. Furthermore, for simulation purposes, the QD array was replaced by an effective layer with the same structure factor as that of the QDs.<sup>20,21</sup> It is important to mention that the relatively broader satellite SL peaks observed in  $\omega$ - $2\theta$  curves (Fig. 1) are caused due to the presence of oppositely strained layers in the SL owing to the strain balancing technique employed during the growth to strain compensate unintentional ZnSe-rich interfacial layer.<sup>13</sup> Also, the surface roughness due to the presence of the QDs contributes to faster dampening of the peak intensities as compared to the simulated curves for an ideal multilayer structure.

The combined thickness of the ZnCdSe spacer and the ZnSe-rich interfacial layer was found out to be  $\sim 2.7$  nm as expected from the growth conditions. The simulation results also gave us the estimation of the compositions of various layers within a SL. These compositions were used to evaluate various material parameters, most importantly valence band offsets<sup>22–24</sup> and heavy-hole effective masses,<sup>24–26</sup> required for the calculations based on the transfer matrix method<sup>27</sup> (TMM).

During RSM studies, various  $\omega$ - $2\theta$  scans were carried out by offsetting  $\omega$  by a small angle to probe along non-zero values of the x-component of the momentum transfer ( $q_x$ ) in addition to the conventional scans along z-component of the momentum transfer ( $q_z$ ). This technique provides information about diffuse scattering due to QDs, which arises from the difference in the scattering factors and the elastic deformation field in the host surrounding QDs, leading to specific size, shape, and position distribution of QDs.<sup>28,29</sup> The RSMs along (002) shown in Figs. 2(a) and 2(b) demonstrate a clear

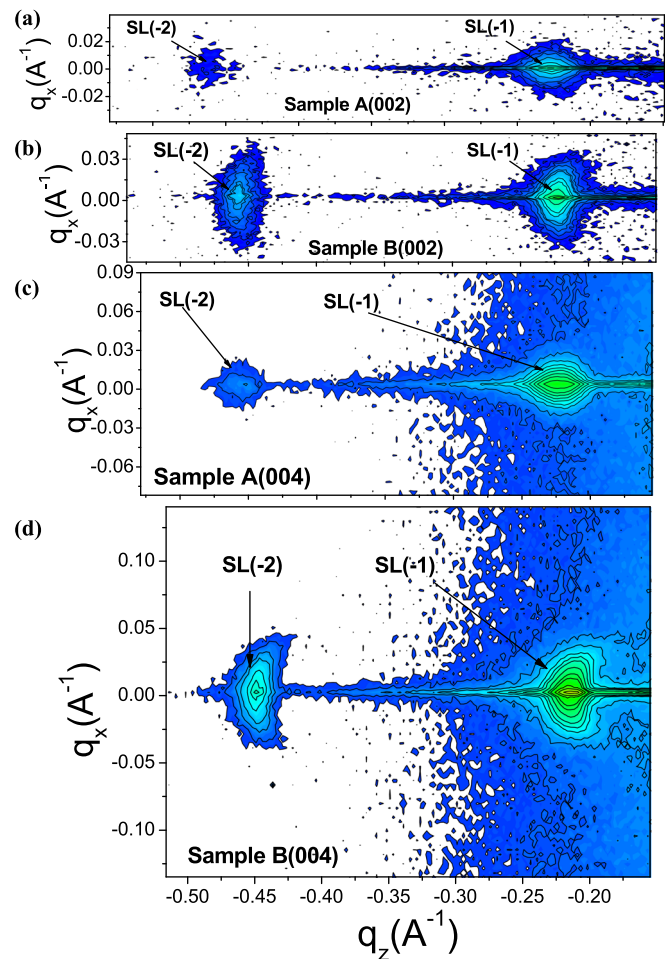


FIG. 2. The RSMs, showing first and second order satellite SL peaks, along (002) reflection: (a) sample A and (b) sample B, and along (004) reflection: (c) sample A and (d) sample B.

elongation in the  $q_x$  direction for the sample with higher Te fraction (sample B). A theoretical explanation derived from a statistical kinematical approach<sup>30</sup> showed that the vertical correlation of QDs manifests itself as a stripe-like feature along the  $q_x$  direction, surrounding the coherent SL peaks and consequently narrowing the width of the diffuse maximum in the  $q_z$  direction. Hence, the most probable explanation for the elongation along  $q_x$  in sample B is enhanced vertical alignment of larger submonolayer QDs, but the effects due to the strain broadening cannot be completely excluded. Thus, to confirm the findings and to eliminate the possibility of the strain broadening, RSMs were measured along (004) reflection and results are shown in Figs. 2(c) and 2(d). The broadening of the diffuse scattering peak related to strain fields surrounding QDs inherently depends on the reciprocal lattice vector  $\mathbf{q}$ , while the elongation of the peak (i.e.,  $\Delta q_x/\Delta q_z$ ) due to vertical alignment of the QDs is independent of  $q$ ,<sup>29,30</sup> and therefore remains the same along both (002) and (004) orientations. The elongation of diffuse scattering peak along (002) reflection was indeed equal to that of along (004) reflection for both the samples, thus, confirming that the source of elongation along the  $q_x$  direction is related to the vertical QD correlation. Such a vertical ordering has previously been observed in other QD structures,<sup>28–33</sup> including submonolayer CdSe/ZnSe QD SLs.<sup>34</sup>

In order to perform detailed structural analysis and to estimate the degree of the vertical QD correlation, a theoretical model given by Kegel *et al.*<sup>32</sup> has been employed. In this model,<sup>32</sup> a Gaussian distribution of horizontal deviations from the underlying dot was assumed for each SL layer. The concept of a mean stacking fault or the standard deviation in the lateral QD position,  $\sigma$ , was developed, which essentially is a measure of average quality of the vertical QD correlation. Also, the form factor and the transmission functions have been neglected in this formalism, as they exhibit a slow variation along  $q_z$ . This model offers a way to estimate the value of  $\sigma$  from half width half maxima (HWHM) along  $q_z$  using following relation:<sup>32</sup>

$$q_z^{HWHM} = \frac{\sigma^2}{D} q_x^2 + \frac{\mu}{D}, \quad (1)$$

where  $D$  is the QD SL period and  $\mu$  is the attenuation factor. If the QD diameter ( $d_{QD}$ ) is known, then using Eq. (1) relative stacking fault,  $f$ , i.e., relative lateral deviation from one dot to the next can also be estimated as

$$f = \frac{\sigma}{d_{QD}} \sqrt{\frac{2}{\pi}} \left( 2 - \frac{\sigma}{d_{QD}} \sqrt{\frac{2}{\pi}} \right). \quad (2)$$

To extract the required parameters in accordance to the earlier discussion, the HWHM along  $q_z$  were then plotted

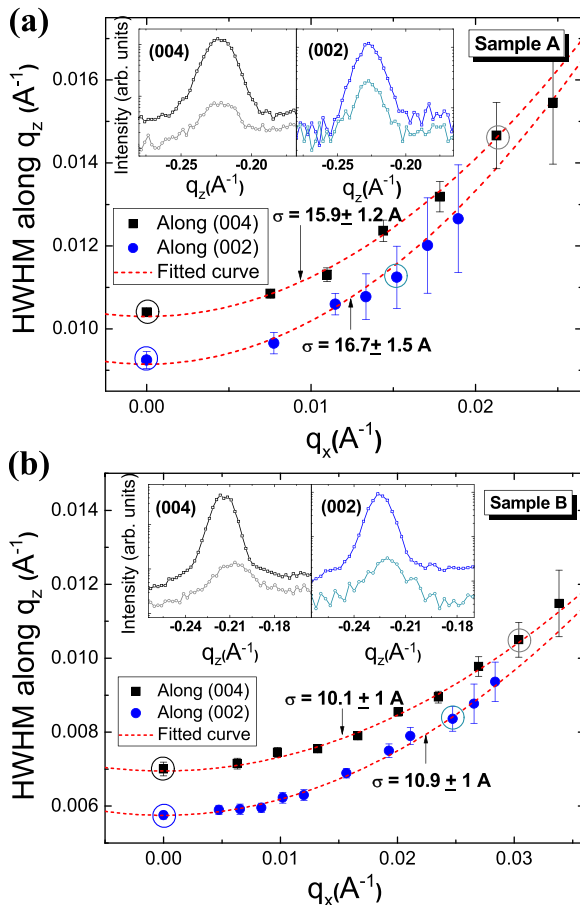


FIG. 3. HWHM along  $q_z$  for SL(-1) along two orientations: (a) sample A and (b) sample B. The dotted lines are the fits using Eq. (1). Insets: The intensity profiles along  $q_z$  for two selected values of  $q_x$ .

against  $q_x$  for the first order satellite SL peak (SL(-1)) of both samples along both orientations as shown in Fig. 3. The experimental data were then fitted using Eq. (1) to determine the value of  $\sigma$  and to estimate  $f$ . An excellent agreement was obtained between the experimental data and the theoretical model, confirming the validity of the model as well as the presence of diffuse scattering from the QD-like centers. The values of  $\sigma$  were found out to be about 16.3 Å and 10.5 Å for samples A and B, respectively. Assuming that the QD size is approximately 15–20 nm, based on the magneto-optical studies<sup>17,35,36</sup> performed on the similar material systems, the average lateral deviation from one dot to another was estimated to be about 13%–17% for sample A and 8%–11% for sample B, indicating enhancement in the vertical QD correlation with the increase in the QD size. This enhanced QD correlation is supposed to increase the QD size uniformity, resulting in a better structural quality and thereby improving the device performance.<sup>37</sup> Most importantly, it gives rise to the formation of a miniband, which was then investigated using optical studies.

The optical characterization of the two samples was performed using CW- and TR-PL in order to probe the effects of the enhanced QD correlation on the optical emission as well as on the radiative lifetimes. The PL spectra of the two

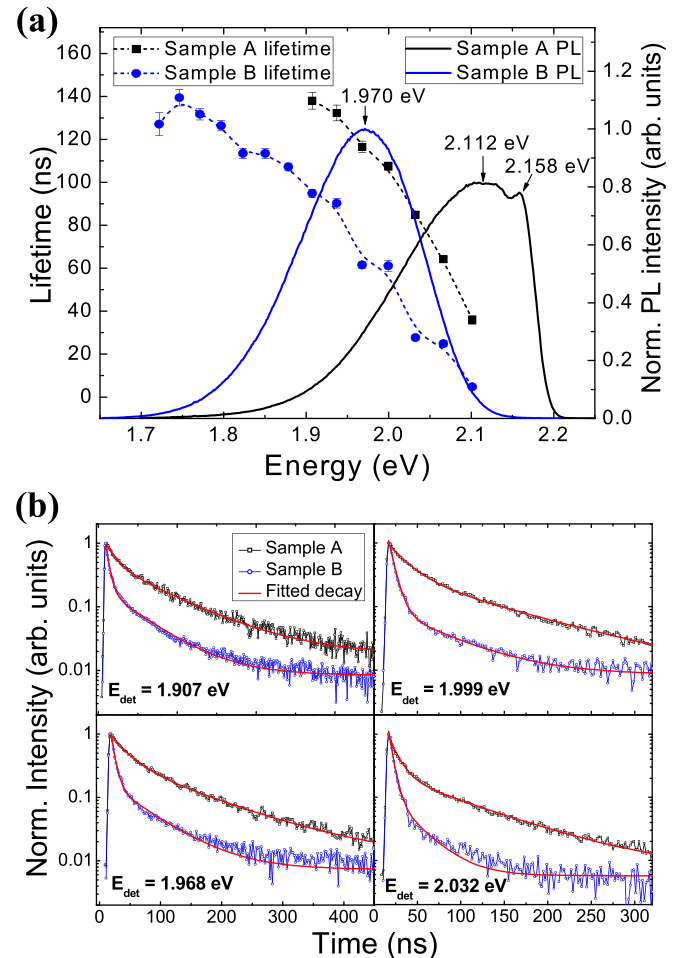


FIG. 4. (a) Solid lines denote the PL spectra normalized to PL peak of sample B and the symbols connected with dotted lines are the extracted radiative lifetime of samples A and B. (b) Experimental and fitted decay curves at various detection energies.

samples are shown in Fig. 4(a) by solid lines, whereas the symbols connected with dotted lines are the extracted radiative lifetimes. It was observed that the PL line width reduced to  $\sim 172$  meV for sample B from  $\sim 197$  meV for sample A. The widths were measured at very low excitation intensities to nullify the effect of band edge excitonic emission related to the spacers. A symmetric and narrower PL spectrum of sample B supports the result of enhanced vertical alignment as the QD correlation is supposed to result in well-arranged QDs leading to smaller size distribution. Moreover, the PL yield obtained in case of sample B was at least 18% more than that of sample A at same excitation intensity (Fig. 4(a)) indicating improved crystalline quality and partial suppression of non-radiative recombinations, thereby pointing towards probable formation of a miniband.<sup>7</sup>

To extract characteristic radiative lifetimes from the TR-PL data, the decay curves were fitted with a double exponential decay (Fig. 4(b)). A rapid decay is observed initially for type-II nanostructures, since the carrier concentration is higher and consequently the electron-hole wavefunction overlap is stronger just after the excitation. However, at longer observation times, these band bending effects become negligible<sup>20,25,38–41</sup> and hence, the actual radiative lifetimes can be extracted. Moreover, in type-II nanostructures, the characteristic lifetime depends on the size of the QDs and therefore on the detection energy, as a result of the variation in electron-hole wavefunction overlap with the change in QD size. Thus, radiative lifetimes were extracted for both the samples from the fitted decay curves at various detection energies and are shown in Fig. 4(a). In spite of larger QDs on average in sample B, it was observed that the radiative lifetimes were much lower than those obtained for sample A at the same detection energies. This can be a result of the overlap between wavefunctions of holes situated in different

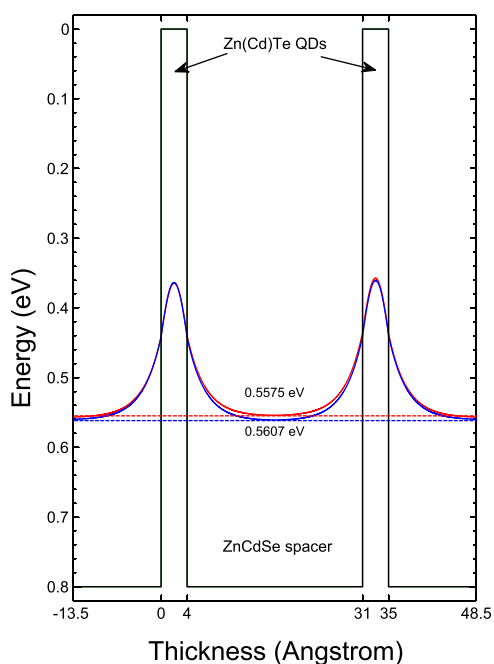


FIG. 5. Calculated, using TMM, energy levels of holes, confined within the 0.4 nm thick Zn(Cd)Te coupled QDs separated by a 2.7 nm thick ZnCdSe spacer. Black solid lines show potential profile whereas red and blue curves are the hole probability densities for each of the two energy levels.

dots separated by a thin spacer especially due to enhanced vertical QD correlation, further hinting to a miniband formation. Similar effects were previously reported for other QD structures.<sup>33,42,43</sup>

In order to further verify the possibility of miniband formation as suggested by the RSM, CW-, and TR-PL results, quantum mechanical calculations were performed using one-dimensional TMM<sup>27</sup> for coupled-QD system, inputting the values of required material parameters preliminary obtained from the HRXRD simulations. The average QD thickness was assumed to be  $\sim 0.4$  nm as estimated from the PL peak position of sample B supposing no electron confinement in the spacers. The TMM results shown in Fig. 5 demonstrate that the hole wavefunctions are no longer localized within a single QD but are shared by all the QDs indicating complete hole coupling. Thus, formation of a miniband is highly probable in a system of fully correlated Zn(Cd)Te QDs separated by 2.7 nm ZnCdSe spacer similar to that of sample B.

In summary, the RSM studies performed on submonolayer Zn(Cd)Te/ZnCdSe type-II QDs along with the theoretical analysis showed the enhancement in the vertical QD correlation with the increase in the QD size. Furthermore, CW-PL and TR-PL, accompanied by the TMM calculations, showed the increased overlap of the wavefunctions for holes belonging to different QDs as a result of increased vertical QD correlation. Thus, QDs with lesser size distribution and possibility of miniband formation in addition to the appropriate material parameters make this material system a potential candidate for a practical IB-SC.

This research was supported by the U.S. Department of Energy, Office of Basic Energy Sciences, Division of Materials Sciences and Engineering under Award No. DE-SC003739. Use of the National Synchrotron Light Source, Brookhaven National Laboratory, was supported by the U.S. Department of Energy, Office of Science, Office of Basic Energy Sciences, under Contract No. DE-AC02-98CH10886.

- <sup>1</sup>A. Luque and A. Martí, *Phys. Rev. Lett.* **78**, 5014 (1997).
- <sup>2</sup>W. Shockley and H. J. Queisser, *J. Appl. Phys.* **32**, 510 (1961).
- <sup>3</sup>G. L. Araújo and A. Martí, *Sol. Energy Mater. Sol. Cells* **33**, 213 (1994).
- <sup>4</sup>A. Luque and A. Martí, *Prog. Photovoltaics* **9**, 73 (2001).
- <sup>5</sup>A. Luque and A. Martí, *Adv. Mater.* **22**, 160 (2010).
- <sup>6</sup>A. Luque, A. Martí, and C. Stanley, *Nat. Photonics* **6**, 146 (2012).
- <sup>7</sup>A. Luque, A. Martí, E. Antolín, and C. Tablero, *Phys. B: Condens. Matter* **382**, 320 (2006).
- <sup>8</sup>A. Luque, A. Martí, N. López, E. Antolín, E. Cánovas, C. Stanley, C. Farmer, L. J. Caballero, L. Cuadra, and J. L. Balenzategui, *Appl. Phys. Lett.* **87**, 083505 (2005).
- <sup>9</sup>A. Martí, E. Antolín, C. Stanley, C. Farmer, N. López, P. Díaz, E. Cánovas, P. Linares, and A. Luque, *Phys. Rev. Lett.* **97**, 247701 (2006).
- <sup>10</sup>A. Martí, N. López, E. Antolín, E. Cánovas, A. Luque, C. R. Stanley, C. D. Farmer, and P. Díaz, *Appl. Phys. Lett.* **90**, 233510 (2007).
- <sup>11</sup>A. M. Kechiantz, L. M. Kocharyan, and H. M. Kechiyants, *Nanotechnology* **18**, 405401 (2007).
- <sup>12</sup>P. G. Linares, A. Martí, E. Antolín, C. D. Farmer, Í. Ramiro, C. R. Stanley, and A. Luque, *Sol. Energy Mater. Sol. Cells* **98**, 240 (2012).
- <sup>13</sup>S. Dhomkar, I. L. Kuskovsky, U. Manna, I. C. Noyan, and M. C. Tamargo, *J. Vac. Sci. Technol. B* **31**, 03C119 (2013).
- <sup>14</sup>S. Dhomkar, U. Manna, L. Peng, R. Moug, I. C. Noyan, M. C. Tamargo, and I. L. Kuskovsky, *Sol. Energy Mater. Sol. Cells* **117**, 604 (2013).
- <sup>15</sup>A. Luque, P. G. Linares, A. Mellor, V. Andreev, and A. Martí, *Appl. Phys. Lett.* **103**, 123901 (2013).
- <sup>16</sup>G. G. Zegrya and A. D. Andreev, *Appl. Phys. Lett.* **67**, 2681 (1995).

- <sup>17</sup>I. L. Kuskovsky, W. MacDonald, A. O. Govorov, L. Mouroukh, X. Wei, M. C. Tamargo, M. Tadic, and F. M. Peeters, *Phys. Rev. B* **76**, 035342 (2007).
- <sup>18</sup>S. Takagi, *Acta Crystallogr.* **15**, 1311 (1962).
- <sup>19</sup>D. Taupin, *Bull. Soc. Fr. Mineral. Cristallogr.* **87**, 469 (1964).
- <sup>20</sup>Y. Gong, W. MacDonald, G. Neumark, M. C. Tamargo, and I. L. Kuskovsky, *Phys. Rev. B* **77**, 155314 (2008).
- <sup>21</sup>U. Manna, I. C. Noyan, Q. Zhang, I. F. Salakhutdinov, K. A. Dunn, S. W. Novak, R. Moug, M. C. Tamargo, G. F. Neumark, and I. L. Kuskovsky, *J. Appl. Phys.* **111**, 033516 (2012).
- <sup>22</sup>J. Puls, M. Rabe, H.-J. Wünsche, and F. Henneberger, *Phys. Rev. B* **60**, R16303 (1999).
- <sup>23</sup>S. Kim, B. Fisher, H.-J. Eisler, and M. Bawendi, *J. Am. Chem. Soc.* **125**, 11466 (2003).
- <sup>24</sup>W. Faschinger, S. Ferreira, and H. Sitter, *Appl. Phys. Lett.* **64**, 2682 (1994).
- <sup>25</sup>V. A. Shuvayev, I. L. Kuskovsky, L. I. Deych, Y. Gu, Y. Gong, G. F. Neumark, M. C. Tamargo, and A. A. Lisiansky, *Phys. Rev. B* **79**, 115307 (2009).
- <sup>26</sup>E. Tyrrell and J. Smith, *Phys. Rev. B* **84**, 165328 (2011).
- <sup>27</sup>B. Jonsson and S. T. Eng, *IEEE J. Quantum Electron.* **26**, 2025 (1990).
- <sup>28</sup>V. Holý, G. Springholz, M. Pinczolis, and G. Bauer, *Phys. Rev. Lett.* **83**, 356 (1999).
- <sup>29</sup>V. Holý, J. Stangl, T. Fromherz, R. Lechner, E. Wintersberger, G. Bauer, C. Dais, E. Müller, and D. Grützmacher, *Phys. Rev. B* **79**, 035324 (2009).
- <sup>30</sup>A. A. Darhuber, P. Schittenhelm, V. Holý, J. Stangl, G. Bauer, and G. Abstreiter, *Phys. Rev. B* **55**, 15652 (1997).
- <sup>31</sup>V. Holý, A. Darhuber, G. Bauer, P. Wang, Y. P. Song, C. M. S. Torres, and M. C. Holland, *Phys. Rev. B* **52**, 8348 (1995).
- <sup>32</sup>I. Kegel, T. Metzger, J. Peisl, J. Stangl, G. Bauer, and D. Smilgies, *Phys. Rev. B* **60**, 2516 (1999).
- <sup>33</sup>S. Maćkowski, G. Karczewski, T. Wojtowicz, J. Kossut, S. Kret, a. Szczepańska, P. Dłużewski, G. Prechtel, and W. Heiss, *Appl. Phys. Lett.* **78**, 3884 (2001).
- <sup>34</sup>I. Krestnikov, M. Straßburg, M. Caesar, A. Hoffmann, U. Pohl, D. Bimberg, N. Ledentsov, P. Kop'ev, Z. Alferov, D. Litvinov, A. Rosenauer, and D. Gerthsen, *Phys. Rev. B* **60**, 8695 (1999).
- <sup>35</sup>I. L. Kuskovsky, Y. Gong, G. F. Neumark, and M. C. Tamargo, *Superlattices Microstruct.* **47**, 87 (2010).
- <sup>36</sup>B. Roy, H. Ji, S. Dhomkar, F. J. Cadieu, L. Peng, R. Moug, M. C. Tamargo, and I. L. Kuskovsky, *Appl. Phys. Lett.* **100**, 213114 (2012).
- <sup>37</sup>W. Liu, H. Wu, F. Tsao, T. Hsu, and J. Chyi, *Sol. Energy Mater. Sol. Cells* **105**, 237 (2012).
- <sup>38</sup>N. N. Ledentsov, J. Böhrer, M. Beer, F. Heinrichsdorff, M. Grundmann, D. Bimberg, S. V. Ivanov, B. Y. Meltser, S. V. Shaposhnikov, I. N. Yassievich, N. N. Faleev, P. S. Kop'ev, and Z. I. Alferov, *Phys. Rev. B* **52**, 14058 (1995).
- <sup>39</sup>F. Hatami, M. Grundmann, N. N. Ledentsov, F. Heinrichsdorff, R. Heitz, J. Böhrer, D. Bimberg, S. S. Ruvimov, P. Werner, V. M. Ustinov, P. S. Kop'ev, and Z. I. Alferov, *Phys. Rev. B* **57**, 4635 (1998).
- <sup>40</sup>Y. Gu, I. L. Kuskovsky, M. van der Voort, G. F. Neumark, X. Zhou, and M. C. Tamargo, *Phys. Rev. B* **71**, 045340 (2005).
- <sup>41</sup>U. Manna, Q. Zhang, S. Dhomkar, I. F. Salakhutdinov, M. C. Tamargo, I. C. Noyan, G. F. Neumark, and I. L. Kuskovsky, *J. Appl. Phys.* **112**, 063521 (2012).
- <sup>42</sup>N. N. Ledentsov, V. A. Shchukin, M. Grundmann, N. Kirstaedter, J. Böhrer, O. Schmidt, D. Bimberg, V. M. Ustinov, A. Y. Egorov, A. E. Zhukov, P. S. Kop'ev, S. V. Zaitsev, N. Y. Gordeev, Z. I. Alferov, A. I. Borovkov, A. O. Kosogov, S. S. Ruvimov, P. Werner, U. Gösele, and J. Heydenreich, *Phys. Rev. B* **54**, 8743 (1996).
- <sup>43</sup>O. L. Lazarenkova and A. A. Balandin, *J. Appl. Phys.* **89**, 5509 (2001).